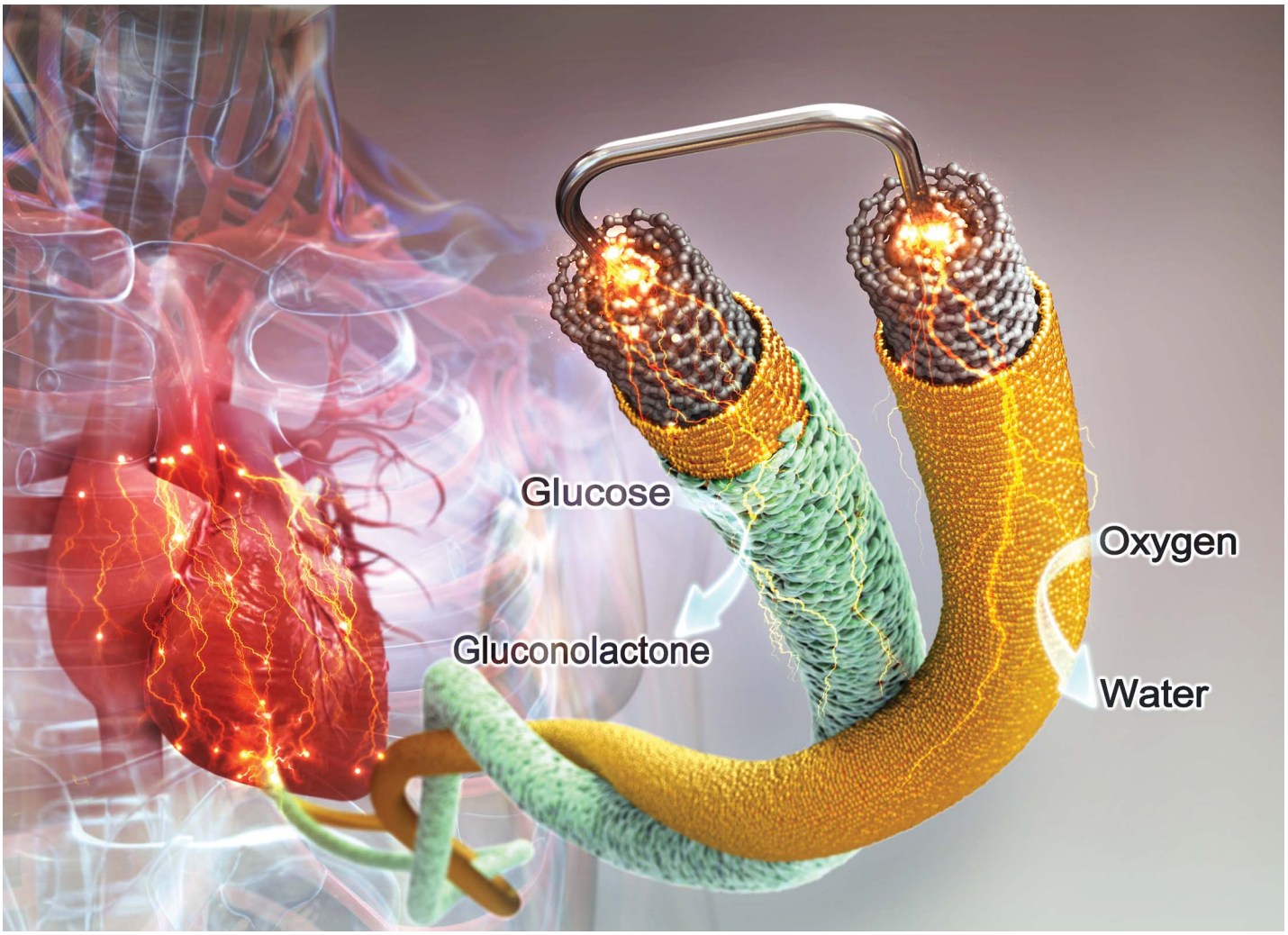

Showcasing a study on Au nanoparticle-coated highly conductive carbon fiber biofuel cell electrodes and their application for powering implanted devices by a group of researchers led by Prof. Jinhan Cho from Korea University and Prof. Seung Woo Lee from Georgia Institute of Technology.

Highly conductive electrocatalytic gold nanoparticle-assembled carbon fiber electrode for high-performance glucose-based biofuel cells

Highly conductive carbon fiber electrodes for high-power glucose-biofuel cells were developed using a layer-by-layer assembly method. Considering that Au nanoparticle-coated carbon fiber electrodes can boost the electrochemical performance of pristine carbon fibers, it can be effectively applied in various electrochemical applications, including sensors or energy storage devices as well as biofuel cells.

As featured in:

See Seung Woo Lee, Jinhan Cho *et al.*, *J. Mater. Chem. A*, 2019, **7**, 13495.

ROYAL SOCIETY OF CHEMISTRY | Celebrating IYPT 2019

rsc.li/materials-a

Registered charity number: 207890

Journal of Materials Chemistry A

PAPER

View Article Online
View Journal | View Issue

Cite this: J. Mater. Chem. A, 2019, 7, 13495

Highly conductive electrocatalytic gold nanoparticle-assembled carbon fiber electrode for high-performance glucose-based biofuel cells†

Cheong Hoon Kwon, [a] Yongmin Ko,[ab] Dongyeeb Shin,[a] Seung Woo Lee *[b] and Jinhan Cho *[a]

Received 22nd December 2018
Accepted 29th March 2019

DOI: 10.1039/c8ta12342j

rsc.li/materials-a

Biofuel cells, which can convert chemical energy into electricity have been considered as one of the most promising candidates for powering implantable and microscale biomedical devices. However, most biofuel cells generate a low power output, limiting their practical applications. Here, we introduce a high-performance biofuel cell based on gold nanoparticle-modified carbon nanotube hybrid fibers. These hybrid electrodes could be converted into anodes through additional enzyme deposition and used directly as cathodes, allowing notable oxygen reduction reaction activity as well as high electrical conductivity (~6100 S cm^{-1}). The formed hybrid biofuel cell, composed of an enzymatic anode and a gold nanoparticle-coated carbon fiber cathode, provides an outstanding stationary power output of 1.2 mW cm^{-2} under a fixed external resistance (cyclic voltammetry measurement ~2.1 mW cm^{-2}) at 300 mmol L^{-1} glucose. Furthermore, these one-dimensional hybrid electrodes with extremely high electrical conductivity can be widely applied in various wire-type electrochemical devices.

1. Introduction

A sustainable power source is a key requirement to support the recent noteworthy advancements in a wide range of electronic devices, including wireless wearable smart sensors and biomedical devices.[1–4] In particular, biofuel cells (BFCs), which are unique for their biocompatibility and operation at mild temperatures and near-neutral pH, are one of the most promising energy sources for powering implantable biomedical devices.[5,6] Despite these notable advantages, compared to other power sources, most BFCs exhibit a low power output (tens to hundreds of μW cm^{-2}),[7,8] which is mainly due to the poor electron transfer between the enzyme and the conductive support. To resolve this critical drawback of BFCs, many efforts have been devoted to improving electron transfer in two different ways: mediated electron transfer (MET) and direct electron transfer (DET) mechanisms. First, MET is based on the use of redox-mediating polymer compounds containing metal ions, such as osmium, ruthenium, and iron.[5,9–12] On the other hand, DET allows electrons to be directly transferred from the active site of the enzyme to the conductive supports such as glassy carbon electrode or graphite electrode, resulting in a relatively low electron transfer efficiency.[13,14] Although MET can provide a much higher current density than DET in BFCs, the toxicity and instability of metal ion-based redox mediators have limited the practical applications of such materials.[15,16] Accordingly, DET-based BFCs (*i.e.*, DET-BFCs) have attracted considerable attention as an alternative that can circumvent the toxicity-related problems of MET-based BFCs.[12,17] However, it should be noted that the electron transfer rate and power output (approximately 10–100 μW cm^{-2}) of DET-BFCs are still substantially inferior to those of MET-BFCs (approximately 100 μW cm^{-2} to 1 mW cm^{-2}).[9,12–14]

As another strategy for overcoming the low power efficiency of DET-BFCs, enzymes such as glucose oxidase (GOx) have been directly deposited onto carbon nanotube fibers (CFs), which are used as conductive supports for BFCs.[9,12,16,17] Despite some improvements in power output through previous CF-based DET-BFCs,[16,17] further improving the performance of DET-BFCs is obviously limited by the low charge-transfer efficiency between the enzyme and the conductive support. Although several other approaches, such as ozone exposure, plasma (*i.e.*, Ar–N_2) treatment, or the decoration of palladium NPs on disk-type carbon nanotube supports, have been proposed to enhance the intrinsic charge transfer kinetics of DET-BFCs, the obtained power output is increased by only approximately two- to three-fold.[18–20] Additionally, most approaches for enzyme immobilization are based on the simple physical adsorption of enzymes onto CFs;[9,12,16,17] this mechanism makes it difficult to exactly control the enzyme thickness, the enzyme conformation, and the interfacial stability between the enzyme and the CF.

[a]Department of Chemical and Biological Engineering, Korea University, 145 Anam-ro, Seongbuk-gu, Seoul 02841, Republic of Korea. E-mail: jinhan71@korea.ac.kr
[b]The George W. Woodruff School of Mechanical Engineering, Georgia Institute of Technology, Atlanta, Georgia 30332, USA. E-mail: seung.lee@me.gatech.edu

† Electronic supplementary information (ESI) available. See DOI: 10.1039/c8ta12342j

This poor control may significantly decrease the utilization of enzymes in electrochemical reactions, thereby restricting the charge transfer kinetics of the electrode.

Electrostatic layer-by-layer (LbL) assembly, which uses well-defined complementary interactions between oppositely charged components in aqueous media, has been considered as the most versatile and effective approach for preparing ultra-thin nanocomposite films with tailored physical and chemical properties.[21–36] As a result, this electrostatic LbL assembly approach has been widely applied to various electrochemical electrodes for energy generation, storage, and conversion devices.[26,28,29] However, in spite of these notable advantages, the traditional electrostatic LbL assembly has much difficulty in preparing highly conductive supports.[30] For example, the sequential LbL assembly of anionic metal NPs and cationic bulky polyelectrolytes in aqueous media results in NP arrays with a low packing density per layer due to the long-range electrostatic repulsion between the same-charged NPs in aqueous media,[31–33] which is closely related to the increase in contact resistance. Additionally, the electrical properties of metal NP multilayers can be strongly restricted by the presence of bulky polyelectrolytes as well as the low packing density of metal NPs.[27,34] Furthermore, in the case of depositing electrostatically LbL-assembled (anionic GOx/cationic polyelectrolyte)$_n$ multilayers onto the conductive supports such as ITO glass for the preparation of glucose-detections sensors or BFCs, the presence of bulky and insulating polyelectrolytes sandwiched between adjacent GOx layers significantly increases the charge transfer resistance of the electrodes.[37]

Here, we introduce a high-performance BFC based on the Au NP-coated CFs (*i.e.*, Au-CFs) with remarkable electrical conductivity and high electrocatalytic activity. To this end, tetraoctylammonium bromide-stabilized Au NPs (*i.e.*, TOABr-Au NPs) with a diameter of ~8 nm were covalently layer-by-layer (LbL)-assembled with amine-functionalized molecule linkers (*i.e.*, tris-(2-aminoethyl)amine (TREN)) onto CFs in organic media. In this case, pristine CFs with an electrical conductivity of approximately 261 S cm^{-1} were converted into Au NP-coated CF electrodes with a low resistivity of ~1.7×10^{-4} Ω cm and a high electrical conductivity of ~6100 S cm^{-1}, which significantly outperforms the electrical conductivity of various modified carbon nanotubes (CNTs) reported to date (*e.g.*, 33 S cm^{-1} for compressed CNT-enzyme electrodes[38]). We also demonstrate that the Au NPs deposited on the CF surface can also act as electron relays for efficient electrocatalytic reactions, and resultantly, highly conductive Au-CF electrode can be directly used as an electrocatalytic cathode that itself enables outstanding oxygen reduction reaction (ORR) activity due to the densely packed but nanoporous Au NP arrays. Additionally, when anionic GOx are electrostatically LbL-assembled with cationic TREN onto the Au-CFs in aqueous media (*i.e.*, GOx/TREN)$_n$ multilayers, the formed electrodes (*i.e.*, GOx/Au-CFs) are used as anodes for BFCs. It should be noted that the use of TREN as a short molecule inker instead of bulky polyelectrolyte linker minimizes the charge transfer resistance of the formed electrode. The complete hybrid BFCs (*i.e.*, Au-CF cathode and GOx/Au-CF anode) prepared from these combined LbL assemblies (*i.e.*, covalent bonding- and electrostatic bonding-induced LbL assembly), exhibit a high power output of 1.2 mW cm^{-2} and excellent operating stability (~85% of the initial power performance after 15 days) under fixed external resistance, which are much higher values than those of the CNT-based BFCs reported to date.

2. Experimental section

2.1. Materials

Multi-walled carbon nanotubes fiber (B-type CNT fiber, here abbreviated as CF), GOx (*Aspergillus niger* (180 U mg^{-1})) were purchased from Taiyo Nissan and Amano Enzyme Inc., respectively. Tetraoctylammonium bromide (TOABr), tris-(2-aminoethyl)amine (TREN, $M_w \sim 146$), poly(ethylene imine) (PEI, $M_w \sim 800$), gold(III) chloride trihydrate ($HAuCl_4 \cdot 3H_2O$, ≥99.9%), and sodium borohydride ($NaBH_4$, 99.99%) were purchased from Sigma-Aldrich.

2.2. Synthesis of TOA-Au NPs

TOABr-stabilized Au NPs were synthesized using a two-phase reaction reported as Brust method.[39] Briefly, 30 mmol per L of gold(III) chloride trihydrate ($HAuCl_4 \cdot 3H_2O$) in de-ionized water (30 mL) and 20 mmol per L of TOABr dispersed toluene (80 mL) were mixed with vigorous stirring at room temperature. Then, 0.4 mol L^{-1} aqueous solution of $NaBH_4$ (25 mL) was added to the above mixture for reduction. After sufficient stirring (approximately 3 h), the aqueous solution was separated from the mixture, and then the remaining toluene solution was repeatedly washed with H_2SO_4 (0.1 mol L^{-1}, 95% purity, Daejung Chemicals) and NaOH (0.1 mol L^{-1}, 97%, Sigma-Aldrich). After the washing steps, the remaining aqueous solution was removed. As a result, we used toluene solution containing TOA-Au NPs for the deposition of TOA-Au NP. The diameter size of TOABr-Au NPs in toluene was measured to be approximately 8 nm.

2.3. Preparation of COOH-functionalized CFs

Pristine CFs with a diameter of 32 ± 0.5 μm and a length of 3 mm were first oxidized by in the mixture of nitric acid (HNO_3, 25 wt%) and sulfuric acid (H_2SO_4, 75 wt%) at 70 °C for 90 min for the preparation of COOH-functionalized CFs (COOH-CF). The electrical conductivity of COOH-CFs was measured to be approximately 261 S cm^{-1}. After surface modification, the COOH-CFs were dipped in the PEI polymer solution (1 mg mL^{-1}) for 30 min for the deposition of TOABr-Au NPs.

2.4. Fabrication of *n*-Au-CF electrodes

The COOH-functionalized CF electrode was dipped in ethanol solution containing amine (NH_2)-functionalized PEI ($M_w \sim 800$; 1 mg mL^{-1}) for 30 min to ensure the sufficient loading amount of Au NPs. It should be noted that the PEI with a large amount of amine (NH_2) groups providing multiple binding sites as well as high affinity for TOABr-Au NPs on the surface of the COOH-functionalized CF, and furthermore PEI has stable hydrogen-bonding interaction with COOH-CFs.[27] The PEI-coated COOH-

CFs were then dipped in TOABr-Au NP solution (10 mg mL^{-1}) for 30 min, and then TOABr-Au NPs-coated-CFs were washed with toluene solvent three times. In this case, bulky TOABr ligands bound to the surface of Au NPs were almost completely replaced by NH_2 groups of the PEI-coated CF due to the high affinity between the bare surface of Au NPs and NH_2 groups of PEI. After this adsorption process, TOABr-Au NP-coated CFs were immersed into the TREN ethanol solution (1 mg mL^{-1}) for 30 min, and then washed with pure ethanol. Similarly, the bulky TOABr ligands were completely replaced by NH_2-functionalized TREN molecules. These deposition processes were repeated until the desired bilayer number was obtained. The formed Au-CFs were used as a cathode as well as a conductive support for anode.

2.5. Fabrication of anodes for BFC

For BFC anode, the Au-CF electrode (*i.e.*, $(TOA\text{-}Au\ NP/TREN)_{20}$-coated CF electrode) was immersed into the enzyme (GOx) solution (5 mg mL^{-1}) for 10 min that is dissolved in phosphate buffer saline (PBS), and then washed with deionized water. After the adsorption of GOx, the GOx-coated CF electrode was dipped into the TREN-dissolved PBS buffer solution for 10 min again, and then washed with deionized water. Using these repeated processes, the formed $(GOx/TREN)_{20}/(TOABr\text{-}Au\ NP/TREN)_{20}$/CF was used as an anode for BFC.

2.6. Fabrication of a complete Au-CF BFC

The top end of 20-GOx/Au-CF anode and 20-Au-CF cathode were cemented to each copper wire using commercial silver paste (ELCOAT P-100 from CANS, South Korea) for the electrochemical measurements. The dried silver paste was further insulated with an epoxy adhesive (5 Minute Epoxy S-208 from DEVCON, USA). After the installation of the anode and the cathode in an electrochemical cell containing 50 mL PBS solution (20 mmol L^{-1} phosphate, 0.14 mol L^{-1} NaCl, pH: ~7.4) at 37 °C, the BFC power densities were determined by two different methods; (1) the cyclic voltammogram (CV) measurement and (2) current flowing measurement through an external variable resistor (in the range of 1 kΩ to 10 MΩ) to control cell potential (see Fig. S1†). Additionally, the toxic chemical issues of toluene, TOABr ligands, and PEI polymers should be considered in view of the biocompatibility of Au-CF electrode. The more detailed explanation is given in the ESI.†

2.7. Measurements

FTIR analysis was carried out using a CARY 600 spectrometer (Agilent Technology) in the specular mode at room temperature, and the obtained dataset was plotted after line smoothing using spectra analyzing software (OMNIC, Nicolet). All spectra were obtained from 200 scans. The loading mass of the $(TOABr\text{-}Au\ NP/TREN)_n$ multilayers adsorbed onto the CF electrode was measured using an analytical balance (XP205 model, Mettler Toledo, resolution of 0.01 mg). For this investigation, we first measured the mass of the pristine CF electrode, and then measured the total mass of $(TOABr\text{-}Au\ NP/TREN)_n$ multilayer-coated CF electrode. Using this measurement, we estimated the mass of $(TOABr\text{-}Au\ NP/TREN)_n$ multilayers adsorbed onto the CF electrodes. The height of $(GOx/TREN)_{20}$ multilayer on Au-coated silicon wafer was scanned using atomic force microscopy (AFM, XE-100, Park Systems) in non-contact mode. The film thickness was also measured by spectroscopic ellipsometry (SE MG-1000, Nano-view Co.) at an incidence angle of 70.5° over five positions on the formed $(GOx/TREN)_m$ multilayer. Surface morphological images and cross-sectional images of Au-CF-based BFC electrodes were investigated using scanning electron microscopy (Hitachi S4700).

For the electrochemical measurements, the top end of an electrode was cemented to a copper wire using commercial silver paste (ELCOAT P-100 from CANS, South Korea). The Au-CF electrode (for cathode) and GOx/Au-CF electrode (for anode) were used as the working electrode, with Ag/AgCl reference electrode and a Pt counter electrode, respectively. A three-electrode electrochemical cell coupled to electrochemical analyzers (an Ivium-n-Stat, Ivium Technologies) was used for cyclic voltammetry and chronoamperometry. Cyclic voltammograms (CVs) of Au-CF-based BFC electrodes were measured in the potential range from −0.6 to +0.6 V in PBS buffer (20 mmol L^{-1} phosphate, 0.14 mol L^{-1} NaCl) of pH 7.4. Nyquist plots of the real and imaginary parts (Z' and Z'') of a hybrid complete BFC were obtained from electrochemical impedance spectroscopy (EIS) measurements in a frequency range from 0.2 Hz to 100 kHz.

3. Results and discussion

3.1. Highly conductive Au-CF electrodes

To prepare the Au-CF electrode, TOABr-stabilized Au NPs (*i.e.*, TOABr-Au NPs) with a diameter of approximately 8 nm (see Fig. S2a†)[39] and TREN (M_w ~ 146, Fig. S2b†) were LbL-assembled onto CFs (*i.e.*, $(TOABr\text{-}Au\ NP/TREN)_n$/CF) with a diameter of approximately 35 μm and a length of 3 mm using the high affinity between the Au NPs and the primary amine (NH_2) moiety of TREN in organic media (Fig. 1a). Although the plasmon absorption peak (λ_{max}) of TOABr-Au NPs dispersed in toluene was located at 523 nm (Fig. S3a†), the absorption peak of $(TOABr\text{-}Au\ NP/TREN)_n$ multilayers was gradually broadened and redshifted to the near-infrared (IR) region upon increasing the bilayer number (n) of multilayers from 1 to 10. Considering that the surface plasmon resonance peak of Au NPs is closely related to the NP–NP distance, these results suggest that the interparticle distance within the Au NPs decreased in both the lateral and vertical dimensions, resulting in the high packing density of the NPs (Fig. S3b†) (more detailed explanation is given in the latter part).

The formation of dense and stable $(TOABr\text{-}Au\ NP/TREN)_n$ multilayers was also confirmed by Fourier-transform infrared (FTIR) spectroscopy in attenuated total reflection (ATR) mode (Fig. S4†). The ATR-FTIR spectra of the TOABr-Au NPs and TREN exhibited distinctive absorption peaks originating from the C–H stretching vibrations of long aliphatic chains at 2928 and 2856 cm^{-1} and the N–H bending vibration of amine groups ($-NH_2$) at 1654 and 1554 cm^{-1}, respectively. Additionally, the C–H scissor peaks (at 1446 cm^{-1}) of the TOABr ligands

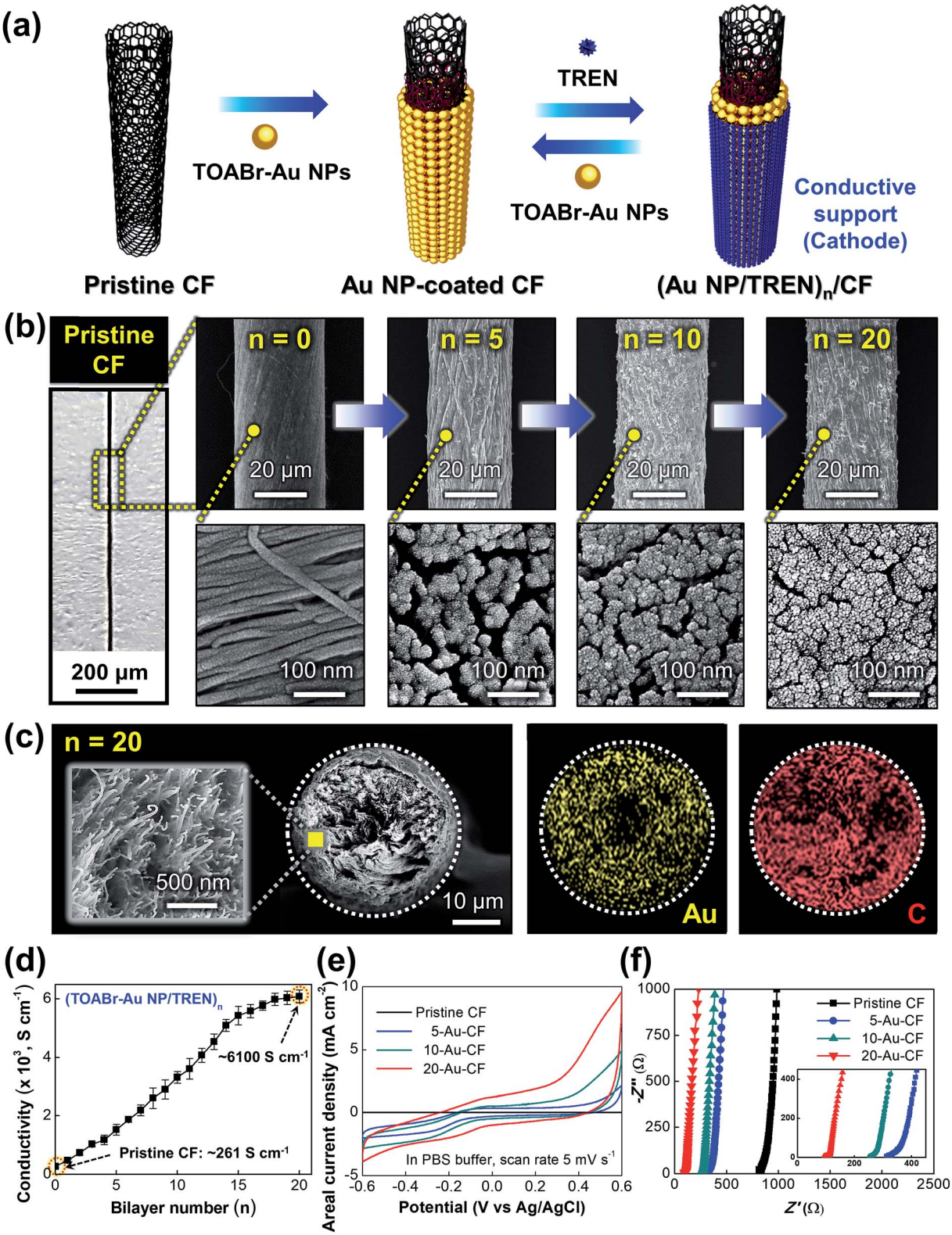

Fig. 1 Characterization of $(TOABr\text{-}Au\ NP/TREN)_n$ multilayers. (a) Schematic design of $(TOABr\text{-}Au\ NP/TREN)_{20}$/CF layer-by-layer (LbL)-assembled carbon fiber (Au-CF) electrodes. Here, n is the number of TOABr-Au NP/TREN layers. (b) Optical image of the pristine CF electrode and surface morphological SEM images of the n-Au-CF electrode with a varying number of TOABr-Au NP/TREN layers ($n = 5$, 10, and 20). (c) SEM cross-section images at low and high magnification of the fracture surface and EDS images of 20-Au-CF (~35 μm diameter), which show porous nanostructures that contain the Au NPs. (d) Electrical conductivity of n-Au-CF as a function of n. (e) Cyclic voltammetry curves of n-Au-CFs at a scan rate of 5 mV s^{-1} in PBS buffer solution. (f) Nyquist plots of n-Au-CFs in the frequency range 0.2 Hz to 100 kHz. The ESR values for $n = 0$, 5, 10, and 20 were 810, 324, 258, and 100 Ω, respectively.

overlapped with the N–H bending vibration of TREN. As the TREN layer was deposited onto the outermost TOABr-Au NP-coated Si substrate (see the absorption spectrum of the 0.5-bilayered film in Fig. S4b†), the absorption peak intensity of C–H stretching vibrations almost completely disappeared. Conversely, the intensity of the $-NH_2$ group peak slightly increased over the same period. The alternating deposition of TREN and the TOABr-Au NPs produced inversely correlated changes in the peak intensities of the N–H bending and C–H stretching frequencies. These results implied that the TOABr ligands (see the C–H stretching vibrations at 2928 and 2856 cm^{-1}) loosely bound to the surface of Au NPs were replaced by the amine ($-NH_2$) groups of TREN (see N–H bending at 1654 and 1554 cm^{-1}) during LbL deposition due to the higher affinity of the bare surface of the Au NPs for the NH_2 groups of TREN. Therefore, the organic layer between adjacent Au NP layers had a thickness of only one TREN molecule, which minimized the separation gap between Au NPs. These results exactly coincide with the changes in the surface plasmon absorption peaks of $(TOABr\text{-}Au\ NP/TREN)_n$ multilayers shown in Fig. S3b.† That is, TOABr-Au NPs are densely adsorbed onto the substrates because there is no electrostatic repulsion between neighboring Au NPs in nonpolar media, which implies the decrease of NP–NP distance in the lateral dimension. Additionally, when the vertically neighboring TOABr-Au NP layers are bridged by small molecule ligands, the bulky TOABr ligands are almost completely replaced by small TREN molecules ($M_w \sim 146$), and therefore only one TREN molecule layer exists between the vertically adjacent Au NP layers. As a result, with increasing the bilayer number (n) up to 10, the optical properties (that is, UV-vis spectra) of the formed $(TOABr\text{-}Au\ NP/TREN)_n$ multilayers were similar to those of bulk Au film.

We also investigated the surface morphologies of $(TOABr\text{-}Au\ NP/TREN)_{n=0,\ 5,\ 10,\ and\ 20}$ multilayer-coated CF electrodes using field-emission scanning electron microscopy (FE-SEM) images. As shown in Fig. 1b, the TOABr-Au NPs were homogeneously and uniformly deposited onto the inner and outer surfaces of CFs without serious NP agglomeration, whereas the formed Au-CFs exhibited microporous (due to CFs) and nanoporous (due to adsorbed Au NPs) structure. In this case, the loading mass of the $(TOABr\text{-}Au\ NP/TREN)_n$ multilayers increased almost linearly from 20 to 80 μg cm^{-1} as the bilayer number (n) increased from 5 to 20 (Fig. S5†). We also estimated the optimal interparticle distance by a density functional theory (DFT) investigation of the thickness of one TREN molecule linker sandwiched between two Au surfaces, where the energetics of the TREN were simulated as a function of the separation distance between Au surfaces. The DFT results suggest that a TREN linker on a flat conformation on the Au surface form a nearly atomic-scale layer between the Au surfaces. The estimated adsorption energy of amine groups of TREN on the single Au surface was 11.1 kcal mol^{-1}, and an optimal separation distance of TREN between Au surfaces was ~7 Å with 31.2 kcal mol^{-1} of the estimated adsorption energy of TREN molecule (Fig. S6†).

To further confirm the uniform and dense deposition of $(TOABr\text{-}Au\ NP/TREN)_n$ multilayers onto CFs, we also examined the cross-sectional structure and atomic characteristics of the Au-CF electrodes with a diameter of 35 ± 0.7 μm using FE-SEM images and energy-dispersive X-ray spectroscopy (EDS) mapping, respectively (Fig. 1c). In this case, the TOABr-Au NPs uniformly and deeply infiltrated into the inner center of the porous CF electrode as well as decorating the outer surface, maintaining the nanoporous structures formed from numerous CNT fibers. These adsorption phenomena were mainly attributed to the LbL assembly method based on 8 nm-sized Au NPs and small-molecule linkers (TREN) in organic media, which was in stark contrast with previous reports that the successive deposition of LbL-assembled polymer films onto porous substrates, such as alumina membranes, could easily fill nanosized holes.[40]

In addition to imparting structural uniqueness, the bridging of neighboring Au NPs by only one TREN layer could significantly reduce the contact resistance due to the minimized separation distance and dense packing. These possibilities are strongly supported by the fact that the electrical conductivity and resistivity of the $(TOABr\text{-}Au\ NP/TREN)_n$ multilayer-coated CFs exceeded those of pristine CFs (Fig. 1d and S7†). Specifically, upon increasing the n of $(TOABr\text{-}Au\ NP/TREN)_n$ from 0 to 20, the electrical conductivity of the LbL-assembled Au-CF electrode significantly increased from 261 to 6100 S cm^{-1}, whereas the resistivity notably decreased from 3.8×10^{-3} (for the pristine CF with $n = 0$) to 1.7×10^{-4} Ω cm (for $n = 20$). Furthermore, considering that Au NPs have electrocatalytic properties for the ORR, the Au-CF electrode itself can be used as an electrocatalytic cathode for hybrid BFCs. To demonstrate this possibility, the electrochemical properties of n-Au-CF [*i.e.*, $(TOABr\text{-}Au\ NP/TREN)_n$-coated CF] electrodes were investigated as a function of n at a scan rate of 5 mV s^{-1} using a three-electrode cell configuration in 20 mmol L^{-1} phosphate buffer saline (PBS) under ambient conditions (*i.e.*, the temperature of the surrounding environment) (Fig. 1e). In this case, the current density of the cyclic voltammetry (CV) curves gradually increased with increasing n. In particular, the cathodic current density of the 20-Au-CF electrode was approximately 664 times higher than that measured with the pristine CFs (*i.e.*, $n = 0$) at −0.6 V (Fig. S8a†). Electrochemical impedance spectra (EIS) also exhibited the lower internal resistance (320 Ω for 5-Au-CF, 250 Ω for 10-Au-CF, and 100 Ω for 20-Au-CF at 1 kHz) for the n-Au-CF electrodes than the pristine CF electrode (810 Ω at 1 kHz) (Fig. 1f and S8b†). These results clearly imply that the electrochemical properties of n-Au-CF electrodes are mainly governed by the properties of the Au NP multilayers rather than by those of the pristine CFs.

Based on these results, we investigated the electrochemical cathodic properties of 20-Au-CF using CV in oxygen-free (N_2-saturated), ambient, and oxygen-rich PBS solutions (Fig. S9a and b†). The cathodic current densities of the Au-CF electrode measured at a potential of −0.6 V in ambient and O_2 conditions were −7.6 and −15.5 mA cm^{-2}, respectively. The normalized current density values were obtained by subtracting the areal cathodic current density at a specific potential of −0.6 V in oxygen-free conditions from the areal cathodic current density measured at the same potential in ambient or oxygen-rich conditions. Here, the normalized current density levels imply that the capacitive and other parasitic currents of the electrode

are eliminated. Therefore, the normalized current predominantly comes from the ORR at the cathode, which is closely related to the stationary power of the BFC, measured by applying a fixed external resistance. On the basis of −3.0 mA cm^{-2}, the value obtained in oxygen-free N_2 conditions, the normalized cathodic current densities at −0.6 V were −4.6 mA cm^{-2} (with an equivalent series resistance (ESR) of 100 Ω) under ambient conditions and −12.5 mA cm^{-2} (with an ESR of 88 Ω) under O_2 conditions (see Fig. S9c†). In addition, the areal current density related to the ORR efficiency of the Au-CF cathode was improved with increasing the rotation speed of a stirring bar in a cell from 0 to 300 rpm (see Fig. S10†). Accordingly, the LbL-assembled Au NP multilayers could be effectively used as ORR catalysts for the BFC system as well as bulk metal-like electron conductors, and furthermore, their electrocatalytic performance could be enhanced by increasing the bilayer number (or loading amount) of Au NPs within the CF electrode.

3.2. GOx/Au-CF anodes

As mentioned earlier, the Au-CF electrode can also be utilized as a conductive support for immobilizing enzymes for the preparation of BFC anodes. To this end, a BFC anode was prepared through the additional deposition of electrostatically LbL-assembled $(GOx/TREN)_m$ multilayers onto the 20-Au-CF (hereafter, 20-Au-CF is designated as Au-CF) (Fig. 2a). However, in the case of LbL assembly using bulky GOx with a size of 6.0 × 5.2 × 7.7 nm^3,[41] the thickness of only one or two bilayers can easily exceed the electron-hopping distance (∼2 nm). Therefore, we delicately adjusted the thickness (or loading amount) of the GOx/TREN multilayers by using the solution concentration- and pH-controlled electrostatic LbL assembly of GOx (5 mg mL^{-1}) and TREN (1 mg mL^{-1}) solution at a human-body-compatible pH of 7.4. First, the pK_a (pH with a degree of ionization of 50%) of carboxylic acid groups within GOx is approximately 4.5, and therefore GOx at pH 7.4 is highly negatively charged. However, TREN has a pK_a of ∼10 and is highly positively charged at pH 7.4. These highly charged GOx and TREN substituents were loaded in extremely low amounts per layer because of the long-range electrostatic repulsion between the two compounds with the same charge.[32,42] When the thickness of GOx multilayers onto the Au-coated Si substrates similar to Au-CFs was measured using cross-sectional FE-SEM, the formed $(GOx/TREN)_{20}$ multilayers exhibited ultrathin film thicknesses of approximately 9 nm (Fig. 2b). Additionally, the film thickness of $(GOx/TREN)_{20}$ multilayers using spectroscopic ellipsometry was also estimated to be approximately 9.8 ± 0.8 nm, which was consistent with that obtained by FE-SEM image within the error range. Furthermore, in the case of AFM measurement, the thickness of the $(GOx/TREN)_{20}$ film is measured to be approximately 10 nm (see Fig. S11†). This ultrathin thickness indicates that the GOx multilayers adsorbed onto the substrates were uniformly and conformally flat, with the thickness of a single GOx layer. That is, the adsorption conformation and thickness of $(GOx/TREN)_m$ multilayers can be effectively controlled for facile electron transfer through the enzyme layers.

On the basis of the LbL-assembled GOx multilayers, we first investigated the electron transfer kinetics at the electrode interface according to the outermost layer of the GOx/TREN multilayers (Fig. 2c and d). Specifically, glucose with hydroxyl groups has a higher affinity (hydrogen-bonding interaction) with NH_2-functionalized TREN than with highly negatively charged GOx at pH 7.4. Therefore, glucose could easily infiltrate into the outermost TREN-deposited multilayers. Notably, the outermost TREN-coated electrode displayed much lower electron transfer resistance than the outermost GOx-coated multilayers despite a further increase in layer number (Table S1† and Fig. 2e). Pardo-Yissar *et al.*[43] also reported that negatively charged $Fe(CN)_6^{3-/4-}$ redox probes could be more easily diffused into the outermost positively charged polyelectrolyte-coated multilayers, showing lower electron-transfer resistance than the outermost negatively charged multilayers. Therefore, our results strongly suggest that the use of a small-molecule linker (TREN) for the construction of GOx multilayers has a negligible effect on the electron transport between the GOx and the conductive support (*i.e.*, Au-CF).

Based on these results, we investigated the anodic current density of $(GOx/TREN)_m$/Au-CF (*i.e.*, *m*-GOx/Au-CF) electrodes at a glucose concentration of 300 mmol L^{-1} in PBS solution under ambient conditions (Fig. 3a and S12†). In this case, the normalized current densities of the *m*-GOx/Au-CF anodes almost linearly increased according to the increase in bilayer number (*m*). In particular, the 20-GOx/Au-CF electrode exhibited the highest value of 31.6 mA cm^{-2} (the 5- and 10-GOx/Au-CF electrodes showed values of 9.2 and 17.8 mA cm^{-2}, respectively). Given that GOx enzymes are electrically insulating, these results clearly show that the conformal coating of ultrathin GOx multilayers on the Au-CF surface can be achieved through LbL assembly, allowing the precise control of electrochemical active GOx loading. Although the ESR and charge transfer resistance (R_{ct}) values increased from 97 to 115 Ω and from 14 to 35 Ω, respectively, upon increasing *m* from 0 to 20 due to the deposition of insulating GOx (Fig. 3b), the electrochemical performance of the *m*-GOx/Au-CF electrodes was more strongly influenced by the optimized GOx thickness than by a slight increase in resistance (Fig. 3a).

We also examined the electrochemical performance of the 20-GOx/Au-CF electrode upon increasing the glucose electrolyte concentration from 0 to 300 mmol L^{-1} under ambient conditions (Fig. 3c and S13, S14†). In this case, the normalized anodic current density of the 20-GOx/Au-CF electrode (*the normalized anodic current density excluded the current density of 20-GOx/Au-CF at 0 mmol L^{-1} glucose (7.5 mA cm^{-2}) from the anodic current density of the 20-GOx/Au-CF electrode at +0.6 V*) was notably increased to approximately 31.6 mA cm^{-2} at a glucose concentration of 300 mmol L^{-1} with a low ESR of 116 Ω as confirmed by EIS. In the case of GOx-free Au-CFs, the anodic current density was gradually increased with increasing the concentration of glucose in PBS, which corresponds to approximately 19% of the anodic performance of 20-GOx/Au-CF (Fig. S15†). These results indicate that the Au-CFs can serve as a promising host for effective loading of the enzyme catalyst (GOx) as well as the co-catalyst for the

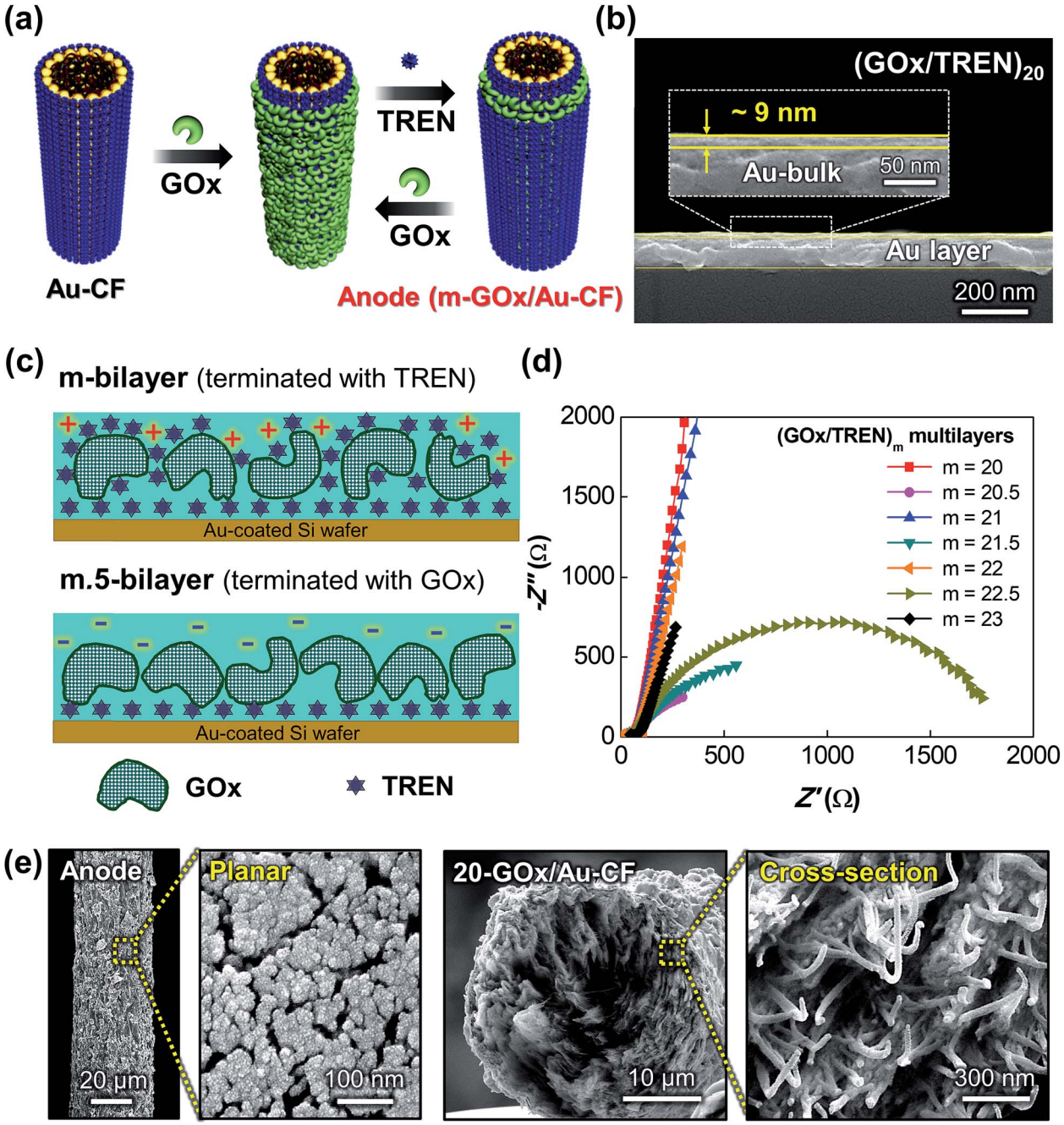

Fig. 2 Characterization of the anode composed of $(GOx/TREN)_m$ multilayers. (a) Schematic illustration of the enzymatic anode assembly process with GOx and TREN on the $(TOABr\text{-}Au\ NP/TREN)_{20}$/CF structure. Here, *m* is the number of GOx/TREN layers. (b) Cross-sectional FE-SEM image showing the film thickness of $(GOx/TREN)_{20}$ multilayers deposited onto a Au-coated Si wafer. (c) Schematic of the outermost layer-dependent interfacial electron transfer kinetics (tested on the Au-coated Si wafer substrate), which are a function of the outermost layer of $(GOx/TREN)_m$ multilayers with different surface charges. (d) Nyquist plots of $(GOx/TREN)_m$ multilayers as a function of bilayer number (*m*). (e) Planar and cross-sectional SEM images at low and high magnification of the 20-GOx/Au-CF anode.

oxidation of glucose. Although a higher glucose concentration increases the electrooxidation reaction involving GOx multilayers adsorbed on Au-CFs, this remarkable increase in the current response of the Au-CF-based anode was closely related to the high electrical conductivity of the Au-CF support. To verify this suggestion, we investigated the electrochemical performance of a pristine CF-based anode (*i.e.*, 20-GOx/CF) under the same experimental conditions (Fig. S16†). In this case, the 20-GOx/CF anode exhibited an extremely low normalized current density of ~2.4 mA cm^{-2} at +0.6 V despite the same enzyme loading as in the 20-GOx/Au-CF anode system. These results clearly demonstrate that the deposition of Au NP multilayers in the CFs allows facile electron transfer between the GOx layer and the conductive support (*i.e.*, Au-

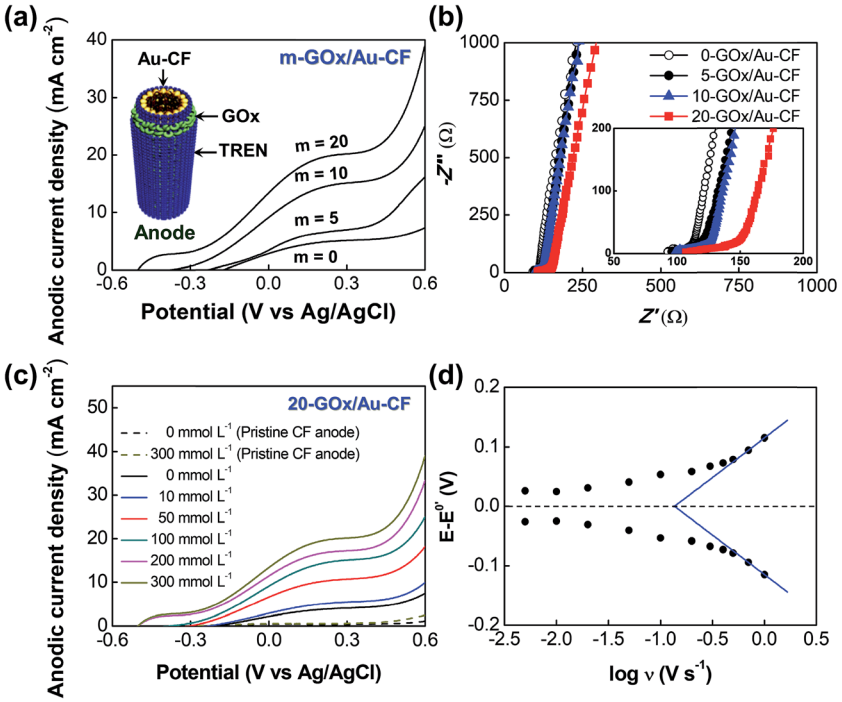

Fig. 3 Electrochemical properties of the BFC anode (*m*-GOx/Au-CF). (a) Anodic current density curves of the $(GOx/TREN)_m$/20-Au-CF electrode. Inset: illustration of anode fibers assembled with *m*-GOx and TREN on 20-Au-CF. (b) Nyquist curves for $(GOx/TREN)_m$/20-Au-CF. The inset shows the high-frequency region. (c) Anodic current density curves of the 20-GOx/20-Au-CF anode as a function of glucose concentration. The areal current density of the 20-GOx/CNT anode was tested and fitted in 0 mmol L^{-1} and 300 mmol L^{-1} glucose buffer conditions for comparison. All measurements were performed at a scan rate of 5 mV s^{-1} in PBS under ambient conditions (a–c). (d) Potential ($E - E^{0\prime}$) *versus* log(ν) measured at a scan rate of 100 mV s^{-1} in PBS under ambient conditions.

CF), resulting in a significantly improved current output (approximately 13 times higher than that of the pristine CF-based anode).

To further investigate the catalytic kinetics of the 20-GOx/Au-CF anode, the apparent heterogeneous electron transfer rate constant (K_s) was estimated using the Laviron method for a quasi-reversible and surface-controlled electrochemical system.[44] Generally, a large K_s indicates a very effective reaction in facilitating the DET of GOx. First, the K_s of the anode was obtained through the plot of separation potential ($\Delta E_p = E - E^0$) *versus* log(ν) in the range of a high scan rate (Fig. 3d and S17†), which was calculated to be $3.5 \pm 0.1\ s^{-1}$. In previous papers, the K_s values for carbon-based electrodes were calculated to be 0.3, 1.53, 3.02, and 2.83 s^{-1} for single-walled nanotube (SWNT)-modified electrodes,[45] multiwalled nanotube (MWNT)-modified electrodes,[46] reduced graphene oxide-MWNT electrodes,[47] and GOx-graphene-chitosan nanocomposite electrodes,[48] respectively. Therefore, it is reasonable to conclude that the DET of Au-CF-based anodes is more favorable than that of conventional carbon-based anodes for BFCs. The surface coverage (Γ) of electroactive GOx can be calculated from the charge integration of the cathodic peak in the CV according to the formula, $\Gamma = Q/nFA$, where Q is the total amount of charge, A is the working electrode area, F is the Faraday constant, and n is the number of electrons transferred ($n = 2$).[49] In this case, the adsorption amount of GOx without the electrocatalytic Au NPs (by the elimination of charge amount originating from GOx-free Au-CF electrode) was estimated to be approximately 3.73×10^{-8} mol cm^{-2}, which was much higher than the GOx loading amount on the glassy carbon electrode (1.17×10^{-10} mol cm^{-2}),[50] and that on the graphene quantum dots modified carbon ceramic electrode (1.80×10^{-9} mol cm^{-2}).[51] In line with these results, it is reasonable to conclude that the notable electrochemical performance of GOx/Au-CF are significantly improved by various positive effects including high electrical conductivity, low charge transfer resistance at the interface between GOx and Au-CF, and high surface coverage of LbL-assembled GOx.

Additionally, the electrochemical response of GOx immobilized onto the heterogeneous surface is mainly due to the redox reaction of electrochemically active sites (flavin adenine dinucleotide, FAD)[52] buried within the enzymes. Here, the small ΔE_p of ~0.11 V obtained from our system indicates a fast heterogeneous electron transfer process, and the reaction was not diffusion-controlled but surface-controlled, as expected for an enzyme-immobilized system. In the case of a surface-controlled system, ΔE_p has been estimated to be less than 200 mV.[53] Therefore, the small ΔE_p (~0.11 V) and large K_s ($\sim 3.5 \pm 0.1\ s^{-1}$) obtained for our GOx/Au-CF anode imply fast electron transfer between the redox center of the enzyme and the surface of the Au-CF electrode. Thus, it was demonstrated that the GOx/Au-CF electrode could be successfully used as a BFC anode with superior electrochemical performance.

3.3. Power output performance

Based on Au-CF-based anodes and cathodes with high electrochemical performance, we prepared a complete hybrid BFC (Fig. 4a and S1†). The power of BFCs can generally be measured by two different methods, CV or varying circuit resistance.[54] First, when the power density of our hybrid Au-CF BFC was measured using polarization tests, the resulting power output was measured to be ~2.1 mW cm^{-2} (with an open-circuit voltage of ~0.98 V) in 300 mmol L^{-1} glucose in ambient conditions. However, the power performance measured by CV

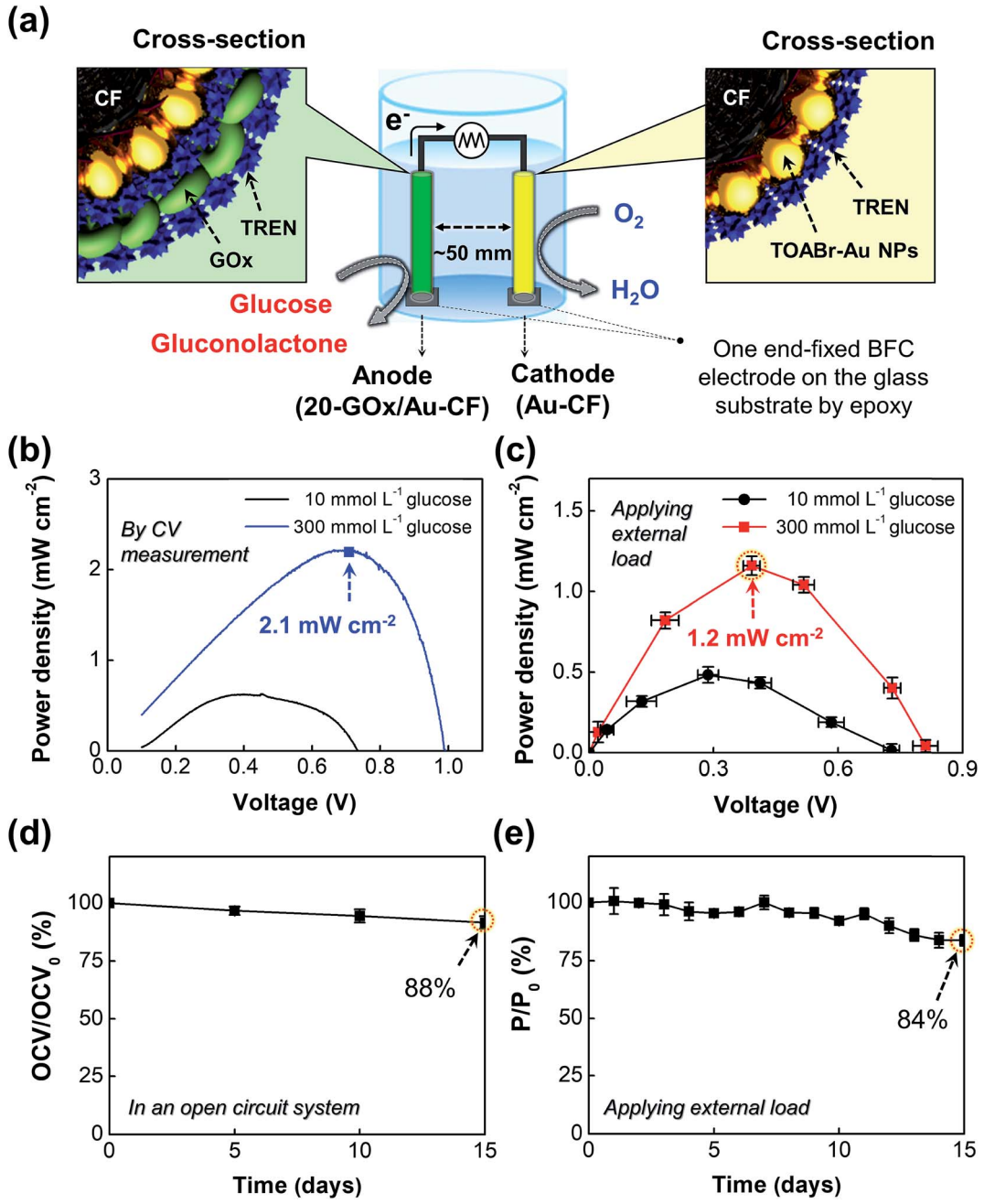

Fig. 4 Performance of hybrid Au-CF-BFCs. (a) Schematic diagram showing the complete hybrid Au-CF-BFC. One end of each BFC electrode was fixed by epoxy on the glass substrate to avoid electrical shortage during continuous operation. (b) Power output of the complete hybrid BFC (consisting of the 20-GOx/Au-CF anode and Au-CF cathode) as a function of potential in 300 mmol L^{-1} glucose in ambient conditions, as obtained by polarization tests. (c) Power output of the complete hybrid BFC upon applying a fixed external resistance in the range of 1 kΩ to 10 MΩ. (D) Voltage (V)–current (I) profiles of the hybrid BFC with different external resistances (1 kΩ to 10 MΩ). All measurements were performed in PBS containing glucose (10 mmol L^{-1} and 300 mmol L^{-1}) under ambient conditions at 37 °C. (d) Relative voltage retention (OCV/OCV_0) of the complete hybrid Au-CF-BFC, measured under an open-circuit system. (e) Relative power retention (P/P_0) of the complete Au-CF-BFC in 10 mmol L^{-1} glucose buffer for 15 days. In this case, the change in the power output of the Au-CF-BFC with external variable resistance was continuously measured as a function of time.

can be overestimated due to the generation of capacitive currents and other parasitic currents (Fig. 4b). To exclude these parasitic currents at the anode and cathode, the transient and stationary power outputs were also measured by applying a fixed external resistance. The resulting areal power density of Au-CF-BFC (composed of 20-GOx/Au-CF) was approximately 1.2 mW cm^{-2} (based on the external surface area of the Au-CF-BFC electrode and corresponding to a volumetric power density of 1325.7 mW cm^{-3} (normalized by total electrode volume) and a length-specific power of 12.8 μW cm^{-1} (normalized by total electrode length)) with an low glucose concentration of 10 mmol L^{-1} (the physiological concentration required for applying the Au-CF-based hybrid BFC in implantable biomedical devices), the BFC exhibited a maximum power density of approximately 0.6 mW cm^{-2} with an open-circuit voltage of ~0.72 V by CV (~0.5 mW cm^{-2} by applying a fixed external load, Fig. 4c and S18†). Furthermore, these high power outputs (~2.1 mW cm^{-2} by CV and ~1.2 mW cm^{-2} by applying a fixed external load) have not been achieved by the conventional carbon-based DET-BFCs reported to date (Table S2†).

These results emphasize the outstanding ability of LbL-assembled Au NP multilayers to minutely regulate the interfacial adsorption onto the CFs and the structure between the Au NPs and GOx, thereby improving the electrochemical performance of the resulting material. As a consequence, the areal power density of the 20-GOx/Au-CF-BFC measured at a fixed resistance was 1.2 mW cm^{-2}, which outperformed the best-reported performance (~0.2 mW cm^{-2})[55] of CNT-based glucose BFCs with DET under a fixed external load. We also confirmed that the developed Au-CF-BFC exhibited good operational stability, maintaining ~88% (~0.63 V) of its initial voltage in an open-circuit system and ~84% (~0.4 mW cm^{-2}) of its initial power density during continuous operation (~15 days) in PBS buffer containing 10 mmol L^{-1} glucose (Fig. 4d, e and S19†). Although the decrease of power output is caused by a few problems such as deactivation of immobilized enzymes (GOx), deactivation of the intrinsic catalytic components, change of the glucose concentration, and partial desorption of GOx from an electrode during the continuous operation of BFC, it should be noted that the operation stability of BFCs shown in our system is very reliable and superior to those of previously reported BFCs.[56,57]

4. Conclusion

We fabricated LbL-assembled hybrid Au-CF electrodes with remarkable electrical conductivity (~6100 S cm^{-1}), high ORR activity, and good operational stability. Additionally, we demonstrated that these Au-CF electrodes could be successfully applied as conductive supports for anodes as well as electrocatalytic cathodes. In particular, an enzymatic anode based on the *m*-GOx/Au-CF electrode could provide a favorable immobilized enzyme conformation as well as effective electron communication between the immobilized enzyme layer and the highly conducive Au-CF electrode, facilitating charge transfer and enzymatic reaction with decreased internal resistance. These improved performances were mainly induced by the stable formation of electrochemically active Au NP arrays and GOx layers using small NH_2-functionalized organic linkers (TRENs). Therefore, under a fixed external resistance, the hybrid BFCs composed of a LbL-assembled 20-GOx/Au-CF anode and 20-Au-CF cathode generated a high-power output with a maximum of 1.2 mW cm^{-2}, which was superior to that of conventional CNT-based BFCs measured under the same conditions (*i.e.*, the use of a fixed external resistor to obtain the power density). Considering that Au-CFs can boost the electrochemical performance of pristine CNTs, we believe that our approach can be effectively applied in various electrochemical applications, including sensors or energy storage devices.

Conflicts of interest

The authors declare no conflict of interest.

Acknowledgements

This work was supported by a National Research Foundation (NRF) grant funded by the Ministry of Science, ICT & Future Planning (MSIP) (2018R1A2A1A05019452; 2016M3A7B4910619) and the Basic Science Research Program through the National Research Foundation of Korea (NRF) funded by the Ministry of Education (NRF-2017R1A6A3A04003192).

Notes and references

1 S. C. Barton, J. Gallaway and P. Atanasov, *Chem. Rev.*, 2004, **104**, 4867–4886.
2 A. J. Bandodkar, J.-M. You, N.-H. Kim, Y. Gu, R. Kumar, A. M. Vinu Mohan, J. Kurniawan, S. Imani, T. Nakagawa, B. Parish, M. Parthasarathy, P. P. Mercier, S. Xu and J. Wang, *Energy Environ. Sci.*, 2017, **10**, 1581–1589.
3 C. Xu, C. Pan, Y. Liu and Z. L. Wang, *Nano Energy*, 2012, **1**, 259–272.
4 S. Shleev, *ChemPlusChem*, 2017, **82**, 522–539.
5 M. Rasmussen, R. E. Ritzmann, I. Lee, A. J. Pollack and D. Scherson, *J. Am. Chem. Soc.*, 2012, **134**, 1458–1460.
6 H. Sakai, T. Nakagawa, Y. Tokita, T. Hatazawa, T. Ikeda, S. Tsujimura and K. Kano, *Energy Environ. Sci.*, 2009, **2**, 133–138.
7 Z. L. Wang and W. Wu, *Angew. Chem., Int. Ed.*, 2012, **51**, 11700–11721.
8 P. Mishra, G. B. V. S. Lakshmi, S. Mishra, D. K. Avasthi, H. C. Swart, A. P. F. Turner, Y. K. Mishra and A. Tiwari, *Nano Energy*, 2017, **39**, 601–607.
9 F. Gao, L. Viry, M. Maugey, P. Poulin and N. Mano, *Nat. Commun.*, 2010, **1**, 2.
10 F. Barrière, Y. Ferry, D. Rochefort and D. Leech, *Electrochem. Commun.*, 2004, **6**, 237–241.
11 F. Zhao, F. Harnisch, U. Schröder, F. Scholz, P. Bogdanoff and I. Herrmann, *Electrochem. Commun.*, 2005, **7**, 1405–1410.
12 C. H. Kwon, S.-H. Lee, Y.-B. Choi, J. A. Lee, S. H. Kim, H.-H. Kim, G. M. Spinks, G. G. Wallace, M. D. Lima, M. E. Kozlov, R. H. Baughman and S. J. Kim, *Nat. Commun.*, 2014, **5**, 3928.

13 K. Murata, K. Kajiya, N. Nakamura and H. Ohno, *Energy Environ. Sci.*, 2009, **2**, 1280–1285.
14 V. Coman, R. Ludwig, W. Harreither, D. Haltrich, L. Gorton, T. Ruzgas and S. Shleev, *Fuel Cells*, 2010, **10**, 9–16.
15 M. Falk, Z. Blum and S. Shleev, *Electrochim. Acta*, 2012, **82**, 191–202.
16 C. H. Kwon, Y. B. Park, J. A. Lee, Y.-B. Choi, H.-H. Kim, R. H. Baughman and S. J. Kim, *RSC Adv.*, 2016, **6**, 48346–48350.
17 F. C. P. F. Sales, R. M. Iost, M. V. A. Martins, M. C. Almeida and F. N. Crespilho, *Lab Chip*, 2013, **13**, 468–474.
18 S. Agrawal, M. S. Raghuveer, H. Li and G. Ramanath, *Appl. Phys. Lett.*, 2007, **90**, 193104.
19 M. Abrar, G. U. Farwa, S. Naseer, A. Saeed, A. W. Khan, Z. Iqbal, S. T. Hussain and M. Zakaullah, *Curr. Appl. Phys.*, 2013, **13**, 567–575.
20 Y.-A. Li, N.-H. Tai, S.-K. Chen and T.-Y. Tsai, *ACS Nano*, 2011, **5**, 6500–6506.
21 G. Decher, *Science*, 1997, **277**, 1232–1237.
22 F. Caruso, R. A. Caruso and H. Möhwald, *Science*, 1998, **282**, 1111–1114.
23 F. Caruso and C. Schüler, *Langmuir*, 2000, **16**, 9595–9603.
24 Y. Ko, H. Baek, Y. Kim, M. Yoon and J. Cho, *ACS Nano*, 2013, **7**, 143–153.
25 Y. Lvov, K. Ariga, I. Ichinose and T. Kunitake, *J. Am. Chem. Soc.*, 1995, **117**, 6117–6123.
26 C. Deng, J. Chen, Z. Nie and S. Si, *Biosens. Bioelectron.*, 2010, **26**, 213–219.
27 Y. Ko, M. Kwon, W. K. Bae, B. Lee, S. W. Lee and J. Cho, *Nat. Commun.*, 2017, **8**, 536.
28 M. N. Hyder, S. W. Lee, F. C. Cebeci, D. J. Schmidt, Y. Shao-Horn and P. T. Hammond, *ACS Nano*, 2011, **5**, 8552–8561.
29 Y. Xiang, S. Lu and S. P. Jiang, *Chem. Soc. Rev.*, 2012, **41**, 7291–7321.
30 J. Cho and F. Caruso, *Chem. Mater.*, 2005, **17**, 4547–4553.
31 N. A. Kotov, I. Dekany and J. H. Fendler, *J. Phys. Chem.*, 1995, **99**, 13065–13069.
32 J. Cho, K. Char, J.-D. Hong and K. Lee, *Adv. Mater.*, 2001, **13**, 1076–1078.
33 J. S. Lee, J. Cho, C. Lee, I. Kim, J. Park, Y. M. Kim, H. Shin, J. Lee and F. Caruso, *Nat. Nanotechnol.*, 2007, **2**, 790–795.
34 Y. Kim, J. Zhu, B. Yeom, M. D. Prima, X. Su, J. G. Kim, S. J. Yoo, C. Uher and N. A. Kotov, *Nature*, 2013, **500**, 59–63.
35 D. Kim, Y. Kim and J. Cho, *Chem. Mater.*, 2013, **25**, 3834–3843.
36 Y. Ko, D. Shin, B. Koo, S. W. Lee, W. S. Yoon and J. Cho, *Nano Energy*, 2015, **12**, 612–625.
37 M. M. Barsan, M. David, M. Florescu, L. Ţugulea and C. M. A. Brett, *Bioelectrochemistry*, 2014, **99**, 46–52.
38 A. Zebda, C. Gondran, A. L. Goff, M. Holzinger and P. C. S. Cosnier, *Nat. Commun.*, 2011, **2**, 370.
39 M. Brust, M. Walker, D. Bethell, D. J. Schiffrin and R. Whyman, *J. Chem. Soc., Chem. Commun.*, 1994, 801–802.
40 J. J. Harris, J. L. Stair and M. L. Bruening, *Chem. Mater.*, 2000, **12**, 1941–1946.
41 S. Libertino, V. Aiello, A. Scandurra, M. Renis and F. Sinatra, *Sensors*, 2008, **8**, 5637–5648.
42 J. Schmitt, G. Decher, W. J. Dressick, S. L. Brandow, R. E. Geer, R. Shashidhar and J. M. Calvert, *Adv. Mater.*, 1997, **9**, 61–65.
43 V. Pardo-Yissar, E. Katz, O. Lioubashevski and I. Willner, *Langmuir*, 2001, **17**, 1110–1118.
44 E. Laviron, *J. Electroanal. Chem.*, 1979, **101**, 19–28.
45 J. Liu, A. Chou, W. Rahmat, M. N. Paddon-Row and J. J. Gooding, *Electroanalysis*, 2005, **17**, 38–46.
46 C. Cai and J. Chen, *Anal. Biochem.*, 2004, **332**, 75–83.
47 V. Mani, B. Devadas and S.-M. Chen, *Biosens. Bioelectron.*, 2013, **41**, 309–315.
48 X. Kang, J. Wang, H. Wu, I. A. Aksay, J. Liu and Y. Lin, *Biosens. Bioelectron.*, 2009, **25**, 901–905.
49 A. J. Bard and L. R. Faulkner, *Electrochemical Methods: Fundamentals and Applications*, John Wiley & Sons, New York, 2nd edn, 2001.
50 J. Zhang, M. Feng and H. Tachikawa, *Biosens. Bioelectron.*, 2007, **22**, 3036–3041.
51 H. Razmi and R. Mohammad-Rezaei, *Biosens. Bioelectron.*, 2013, **41**, 498–504.
52 H. J. Hecht, H. M. Kalisz, J. Hendle, R. D. Schmid and D. Schomburg, *J. Mol. Biol.*, 1993, **229**, 153–172.
53 M. Zhao, Y. Gao, J. Sun and F. Gao, *Anal. Chem.*, 2015, **87**, 2615–2622.
54 C. Feng, Z. Lv, X. Yang and C. Wei, *Phys. Chem. Chem. Phys.*, 2014, **16**, 10464–10472.
55 A. S. Campbell, Y. J. Jeong, S. M. Geier, R. R. Koepsel, A. J. Russell and M. F. Islam, *ACS Appl. Mater. Interfaces*, 2015, **7**, 4056–4065.
56 B. Reuillard, A. L. Goff, C. Agnès, M. Holzinger, A. Zebda, C. Gondran, K. Elouarzaki and S. Cosnier, *Phys. Chem. Chem. Phys.*, 2013, **15**, 4892–4896.
57 H. J. Sim, D. Y. Lee, H. Kim, Y.-B. Choi, H.-H. Kim, R. H. Baughman and S. J. Kim, *Nano Lett.*, 2018, **18**, 5272–5278.